Desalination and Water Treatment

UV-assisted photocatalytic synthesis of TiO$_2$-reduced graphene oxide with enhanced photocatalytic activity in decomposition of sarin in gas phase

R.M. Mohamed [a b c]

[a] Chemistry Department, Faculty of Science, King Abdulaziz University, P.O. Box 80203, Jeddah, 21589, Saudi Arabia

[b] Advanced Materials Department, Central Metallurgical R&D Institute, CMRDI, P.O. Box 87, Helwan, Cairo, 11421, Egypt

[c] Center of Excellence in Environmental Studies, King Abdulaziz University, P.O. Box 80216, Jeddah, 21589, Saudi Arabia Phone: Tel. +966 540715648 Fax: Tel. +966 540715648

PLEASE SCROLL DOWN FOR ARTICLE

UV-assisted photocatalytic synthesis of TiO2-reduced graphene oxide with enhanced photocatalytic activity in decomposition of sarin in gas phase

R.M. Mohamed

Chemistry Department, Faculty of Science, King Abdulaziz University, P.O. Box 80203, Jeddah, 21589, Saudi Arabia
Advanced Materials Department, Central Metallurgical R&D Institute, CMRDI, P.O. Box 87, Helwan, Cairo, 11421, Egypt
Center of Excellence in Environmental Studies, King Abdulaziz University, P.O. Box 80216, Jeddah 21589, Saudi Arabia
Tel. +966 540715648; Fax: +966 2 6952292; email: rmohamedy@cmrdi.sci.eg

ABSTRACT

TiO2-reduced graphene oxide (RGO) composite are successfully prepared by UV-assisted photocatalytic reduction of graphite oxide by TiO_2 nanoparticles in ethanol. These nanocomposites prepared with different ratios of graphene oxide (GO) were characterized by scanning electron microscopy, transmission electron microscopy, X-ray diffraction spectroscopy, UV–vis absorption spectrophotometer (UV–vis), and X-ray photoelectron spectroscopy. Photocatalytic degradation of nerve agent, isopropyl methylphosphonfluroride, Sarin (GB) as a real Chemical Warfare Agent on nanocomposites have been studied using Gas chromatography/mass spectrometry analysis in ambient atmosphere. RGO-TiO_2 nanocomposites exhibited much higher photocatalytic activity than TiO_2 for degradation of GB under visible light irradiation.

Keywords: Graphene oxide; TiO_2; Visible photocatalyst; Nerve agent

1. Introduction

In recent years, photocatalysis has attracted attention as a low cost, environmentally benign method, and detoxification for chemical warfare agents (CWA) has been studied using this high technology. Titanium dioxide (TiO_2) is known to be good photocatalyst for the degradation of environmental contaminants due to its high photocatalytic activity [1–4].

In the past few decades, doping with metal ions, coupling with a second semiconductor, and anchoring TiO_2 particles onto large-surface-area materials, such as mesoporous materials, zeolites or carbon-based materials, have all been elucidated as efficient techniques to improve the photodegradability of semiconductor oxide photocatalysts [5–7]. Among them, TiO_2/carbon nanotube composites have been established as viable potential photocatalysts for use in both water and air purifications [8–10]. The synergetic effect of carbon nanotubes on photocatalyst enhancement, in which carbon nanotubes act as the electron sink for the hindrance of charge carrier recombination [8] or as the photosensitizer to generate a greater density of electron/hole pairs [9], has been previously demonstrated. These TiO_2–nanocarbon composite exhibited higher photocatalytic performance than that of bare

TiO$_2$. However, some problems still hinder further promotion of efficiency of TiO$_2$–nanocarbon composites, such as the weakening of light intensity arriving at surface of catalysts and the lack of reproducibility due to the preparation and treatment variation [11].

Graphene is a new star on applications of condensed-matter physics, electronics, and material science after carbon nanotube and C$_{60}$ [12]. Because graphene is a single-atom thick sheet arranged by sp^2-bonded carbon atoms in a hexagonal lattice, which shows outstanding mechanical, thermal, optical, and electrical properties. Therefore, the interesting graphene-based materials have been extremely extended to application in diverse fields such as nanoelectronic devices, biomaterials, intercalation materials, drug delivery, and catalysis [13–18]. Nanocarbon materials such as carbon nanotube (CNT) and C$_{60}$ have some beneficial effects on the photocatalytic activity of homogeneous and heterogeneous semiconductors by effective electron transfer and interaction effects [19–21]. Among the various semiconductors, titanium dioxide (TiO$_2$) is known to be good photocatalyst for the degradation of environmental contaminants due to its high photocatalytic activity [3,4]. In comparison with CNT and C$_{60}$, graphene has perfect sp^2-hybridized two-dimensional carbon structure with better conductivity and larger surface area, it seems reasonable to envision that the novel graphene–TiO$_2$ nanocomposite with high interfacial contact and potential could be much more promising to improve the photocatalytic performance of TiO$_2$. Furthermore, graphene is easy to produce from inexpensive natural graphite through intermediates product "graphite oxide" [22,23]. The presence of oxygen-containing functional groups in GO and reduced GO makes them as excellent supporters to anchor TiO$_2$ nanocrystals for the synthesis of graphene-TiO$_2$ [24,25]. Recently, graphene/TiO$_2$ composites have been successfully fabricated by various ways. Liang et al. reported that graphene/TiO$_2$ nanocrystals hybrid has been prepared by directly growing TiO$_2$ nanocrystals on GO sheets. The direct growth of the nanocrystals on GO sheets was achieved by a two-step method, in which TiO$_2$ was first coated on GO sheets by hydrolysis and crystallized into anatase nanocrystals by hydrothermal treatment in the second step [24]. Liu et al. prepared the self-assembly of TiO$_2$ with graphene composites in the stabilization of graphene in aqueous solution by assistance of anionic sulfate surfactant [26]. Chen et al. prepared a visible-light responsive GO/TiO$_2$ composite with p/n heterojunction by adding sodium dodecylsulfate in an aqueous of TiCl$_3$ and GO, in which TiO$_2$ could be excited by visible light with wavelengths longer than 510 nm [27].

Some people synthesized graphene/TiO$_2$ composites using GO and P25 as reactants by a facile one-step hydrothermal method and obtained higher photocatalytic activity [28,29].

In this study, a UV-assisted photocatalytic reduction of graphite oxide by TiO$_2$ nanoparticles in ethanol is reported. The photocatalytic activity of the reduced graphene oxide (RGO)–TiO$_2$ nanocomposites is assessed by examining the degradation of real Sarin (GB) from gas phase as a probe reaction under visible light irradiation.

2. Experimental

2.1. Catalysts preparation

2.1.1. Materials

Graphite powder (purity 99.999%); anhydrous ethanol; sodium nitrate; potassium permanganate; titanium tetrachloride (TiCl$_4$), titanium teterisoperpoxide (TTIP); and ethanol (EtOH) were obtained from Sigma-Aldrich. GB has a purity >99%, this agent has high toxicity; it should be handled only by trained personnel using applicable safety procedures.

2.1.2. Synthesis of GO

GO was synthesized by the oxidation of graphite powder using Hummers method [11]. The details are the following: 1 g graphite powder was added in concentration H$_2$SO$_4$ (30 mL) and 1 g NaNO$_3$ solution at 0 °C. While maintaining vigorous stirring, 3 g (1.9 × 10^{-2} mol) KMnO$_4$ was slowly added to the above mixture and left to warm to room temperature. The mixture was continuously stirred at 30 °C until it became pasty brownish, followed by slow addition of deionized water (60 mL), which produced a rapid increase in solution temperature up to a maximum of 90 °C. Then the resultant bright-yellow suspension was terminated by the addition of more distilled water (150 mL), followed by a hydrogen peroxide solution (H$_2$O$_2$, 35 wt.%, 3 mL). The mixture was centrifuged and washed in succession with 200 mL of 1:10 HCl solution, and water until pH = 7. The powder was dried at room temperature under vacuum condition.

2.1.3. Synthesis of titania (T)

At room temperature, a TiCl$_4$/TTIP solution was prepared by dropping TiCl$_4$ (0.6 mL) and TTIP (3 mL) into EtOH (5.0 mL) under vigorous stirring for 10 min. After stirring the resulting mixture for 24 h at room temperature, a semi-transparent sol was obtained. The

sol was subjected to hydrothermal treatment at 160°C for 48 h at a heat rate of 2°C/min. The resulting hydrogel was dehydrated slowly at 40°C for 24 h, 60°C for 12 h, and 80°C for 12 h, successively, until a complete gel particulate was formed. Titania nanoparticles were obtained after thermal treatment at 100°C for 24 h.

2.1.4. Synthesis of RGO/T composites

A certain amount of 4 mg/ml GO and 1 g T nanoparticles was dispersed in 60 mL ethanol and sonicated for 30 min to produce uniform dispersion. UV-assisted photocatalytic reduction of GO by T nanoparticles in ethanol was carried out in a 100 mL cylindrical quartz glass vessel using a 250 W high pressure Hg lamp with the main wave crest at 254 nm for about 24 h under ambient conditions and magnetic stirring. After UV irradiation, it was obviously found that the color of suspension had changed into grayish-black, indicating the successful chemical reduction of GO sheets [30]. The as-synthesized T-RGO samples with 0.4, 0.8, 1.2, 1.4 wt.% RGO, named as TG-1, TG-2, TG-3, TG-4 were isolated by filtration, washed thrice with distilled water, and finally dried in a vacuum oven at 60°C for 24 h. Finally, the obtained samples were calcined at 400°C for 4 h under argon.

2.1.5. Synthesis of T and RGO/T composites plates

The T plate was prepared as follows: T (0.01 g) was dispersed in 40 mL of distilled water and spread on glass plate (5 cm × 5 cm), which was heated on a hot plate (about 80°C). Distilled water was evaporated and thus T was immobilized on glass-plate.

The same method is applied to prepare RGO/T composite plate.

2.2. Characterization and properties

The crystal structures of the resulting products were characterized by X-ray power diffraction (XRD, Bruker advance-D8 power diffractometer with Cu Ka radiation, $\lambda = 0.154178$ nm at 40 kV and 100 mA flux). The morphologies and compositions of the resulting products were studied by transmission electron microscopy (TEM, JEOL JEM-2100 Japan), scanning electron microscope (SEM) images were taken with a Hitachi S-4800 microscope, X-ray photoelectron spectroscopy (XPS) measurements were performed using an ESCALab220i-XL probe (VG Scientific) with monochromated Al Kα radiation (hv = 1486.6 eV). Analysis was carried out in a vacuum chamber ($<2 \times 10^{-9}$ mbar). Peak fittings and deconvolution were performed using the Eclipse (VG Scientific software). Specific surface areas of the samples were measured by Brunauere-Emmette-Teller (BET) method on a Surface Area Analyzer (NOVA2000e, USA) at 77 K through N_2 sorption. The samples were dried at 100°C for 24 h and then degassed at 150°C for 12 h prior to determination. The UV–vis reflectance of the catalysts was measured by diffuse reflectance spectroscopy using a (Perkin Elmer, Lamba 35) instrument. Emission spectra were recorded on FLS 920 spectrofluorometer.

2.3. Photocatalytic reaction

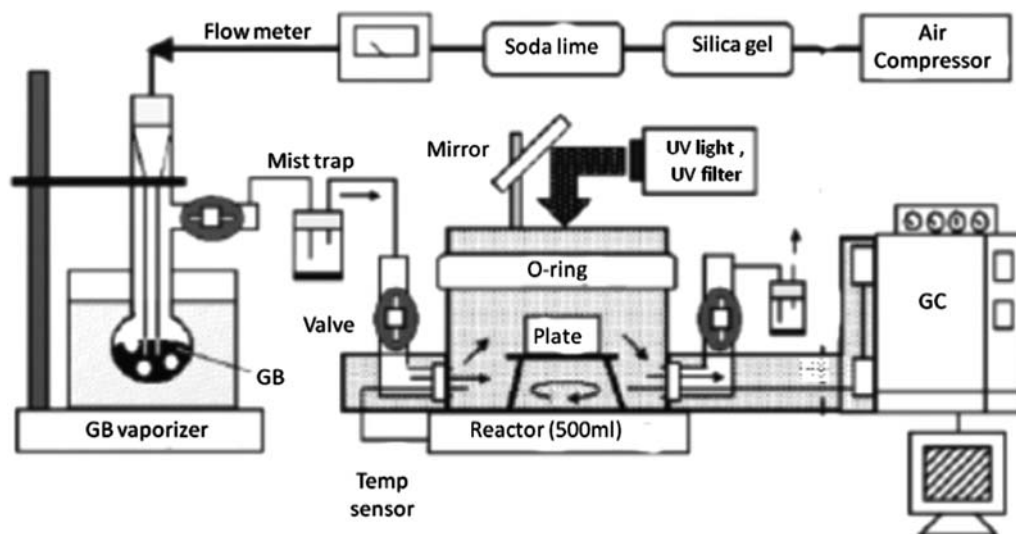Fig. 1 shows a schematic diagram of the photocatalytic-reaction system for GB analysis in the gas phase.

Fig. 1. Diagram of GB photocalytic reaction and analysis system.

Air supplied by the compressor was dried with silica gel, let through a soda lime container to remove CO_2, and bubbled into GB/hexane solution. The vaporized GB was passed through mist trap to remove aerosol and introduced into a 500-mL Pyrex-glass reactor, where a T-plate or T/RGO plate was placed. Teflon stage, O-ring and tube were used for all connections and inner wall of the reactor was treated by silane application in order to decrease adsorption of GB at inner wall of experimental systems. In this study, the GB concentration was basically adjusted by diluting with hexane as solvent. The residual concentration of the vaporized GB in the photocalytic reactor was then 0.5 μmol. The GB/hexane solvent was injected into a glass tube (volume of 500 mL, GL science) equipped with a gas flow cock and was completely vaporized by heating the GB liquid spot in the tube with a heat blower from outside. Then, the temperature in the glass tube was usually 334 K. The vaporized GB/hexane in the glass tube was pumped into the photocatalytic reactor by an air cylinder at a flow rate of 200 mL/min for 2 min. The exhaust cock of the gas pipe in the reactor was then opened in order to keep the pressure of the photocatalytic reactor. After pumping, the inlet and exhaust cocks of the gas pipe in the photocatalytic reactor part were closed. The photocatalysis started after observing the adsorption of the vaporized GB at the surface of T or RGO/T in the dark. Visible irradiation was carried out by Black light (150 W, center wavelength 364 nm) doubly covered with a UV cut filter. The intensity data of UV light are confirmed to be under the detection limit (0.1 mW/cm^2) of a UV radiometer. All of experiments were carried out in ambient air. Gas chromatograph GC-2014 (GC; Shimadzu Co., Kyoto, Japan) was used to analyze GB decrease in the reactor. Sample gas in the reactor was injected automatically through the stainless steel pipe connected directly with the reactor. Organic compounds and phosphoric compounds were detected by flame ionization detector and flame phosphorus detector, respectively. The gaseous products generated by GB photooxidation were analyzed by gas-chromatography–mass spectrometry GC–MS-QP2010 (GC–MS; Shimadzu Co.). Analytical data from the control unexposed to visible light show that no dark degradation or hydrolysis of GB occurs. The decontamination rate was calculated as the percentage of compound consumed from the initial quantity. Caution: GB as CWAs is highly toxic by both inhalation and ingestion. The compounds should always be handled with special care in a special experimental room under reduced air pressure and should be immediately destroyed with sodium hypochlorite after use.
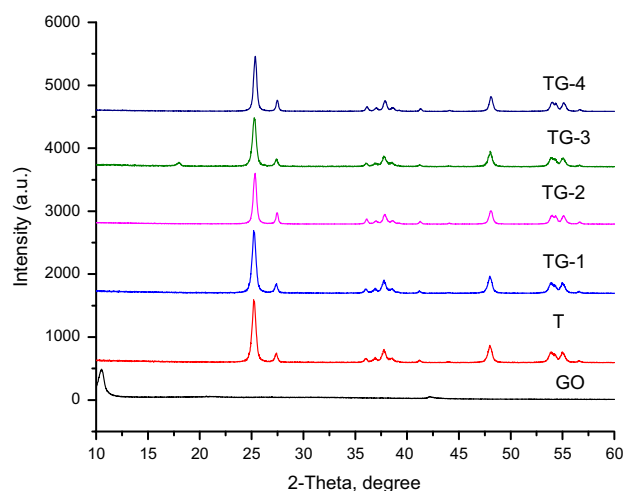

Fig. 2. XRD patterns of the prepared samples.

3. Results and discussion

3.1. Spectral and morphological properties

Fig. 2 shows XRD patterns of GO, T, TG-1, TG-2, TG-3 and TG-4. All of the diffraction peaks match the standard data for pure anatase phase (JCPDS No. 21-1272) of TiO_2, the characteristic peak of GO disappeared in XRD pattern of the composites, revealing that GO was reduced by UV-light at room temperature. What is more, the peak belong to the graphite was also absent in the composites, indicating the decoration of TiO_2 onto graphene sheets caused the enlargement and disorder the layer of graphene.

Fig. 3 shows the SEM images of TG composites. The results reveal that the density of TiO_2 nanocrystals coated on graphene was controlled by the feed ratio of GO/TiO_2, decreasing as the amount of GO increased (Fig. 3).

Fig. 4 shows the EDX spectra of TG-3. The results show the presence of C, O and Ti in TG-3 which confirm the formation of TiO_2–RGO composite.

Fig. 5 shows TEM images of GO, T, and TG composites synthesized with different amounts of GO. As shown in Fig. 5(a), the prepared TiO_2 was spheres with diameter of 90 nm, composing of smaller particles. The introduction of GO to the synthesis system caused the formation of TG composites. As for TG-1 (Fig. 5(b)), TiO_2 nanoparticles with the size of about 35 nm were thickly covered on graphene sheet, some of them aggregated to some extent. In TG-2, the increased amount of GO in reaction system led to the homogeneously scattering of TiO_2 particles on graphene sheet without apparent aggregation, the size of TiO_2 particles decreased slightly to 30 nm. As for TG-3, which was synthesized by further increase the
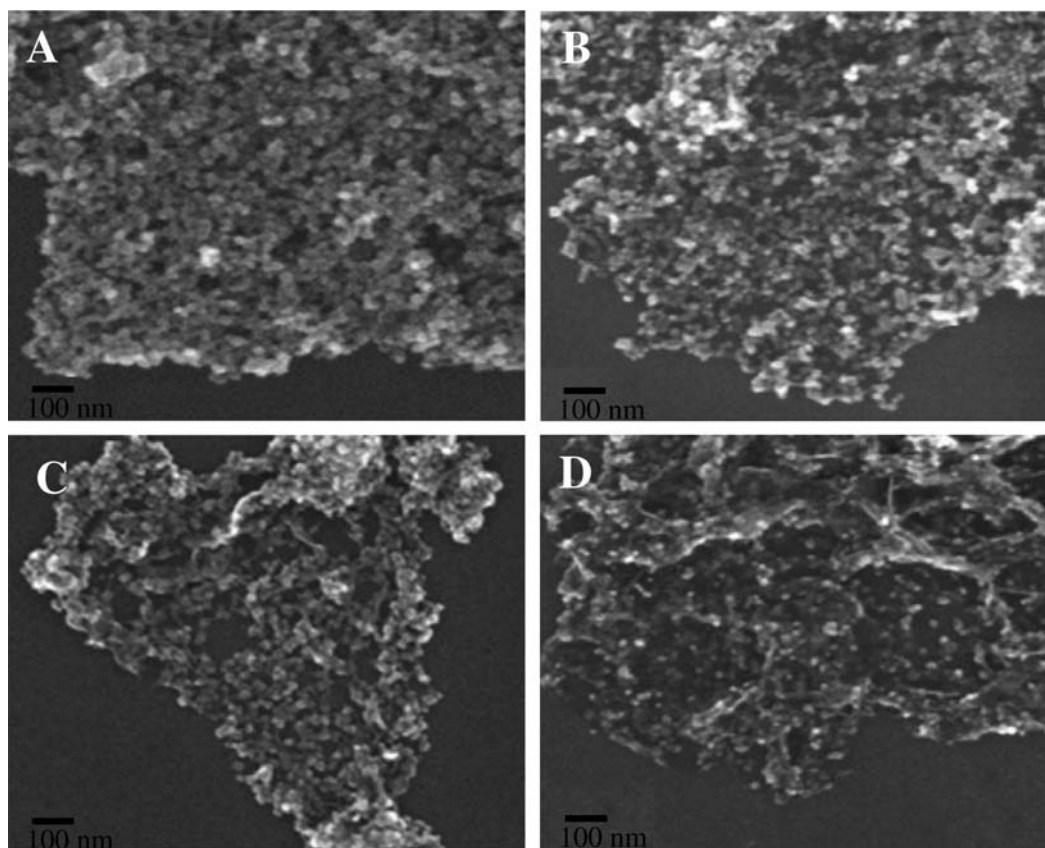
Fig. 3. SEM images of TiO$_2$–RGO composite formed with various GO wt.%: (A) 0.4, (B) 0.8, (C) 1.2, (D) 1.4.

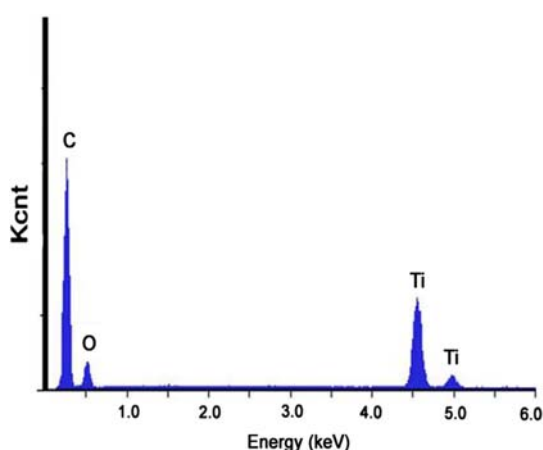
Fig. 4. EDX elemental microanalysis of TG-3.

amount of GO, the formed TiO$_2$ particles with dramatically reduced size of 23 nm were homogeneously and densely scattered on graphene sheet, and the wrinkles of graphene could also be clearly observed. In TG-4, further increase the GO amount, the density of the covered TiO$_2$ particles decreased, the size of

TiO$_2$ is 19 nm. All of the TEM images reveal that the oxygen containing groups in GO can act as anchoring sites to govern the size and dispersity of TiO$_2$, proper amount of GO (1.2 wt.%) in the reactant mixture favors the homogeneous scattering of TiO$_2$ on graphene sheet with smaller size, proper density, and better dispersity, which will further determine the photocatalytic activity of TG composites.

The information regarding the chemical and bonding environment of the graphene matrix and TiO$_2$ phase were ascertained using XPS (Fig. 6). The binding energies (BE) of Ti 2p3/2 and O 1s are 459.1 and 530.0 eV, respectively, which are identical to those for pure TiO$_2$. With respect to the XPS spectra of O 1s, four peaks at 530.4, 531.3, 532.17, and 533.77 eV have been fitted, which are ascribed to Ti–O–Ti (lattice O), C O (and COO), Ti–OH, and C–OH (and C–O–C) species, respectively [31,32]. The main C 1s peak is dominated by elemental carbon at 284.6 eV, attributed mainly to sp^2 hybridized carbon (BE = 284.6 eV). The weak C 1s peak at 285.2 eV is attributed mainly to sp3 hybridized carbon, and two weak peaks at 286.3 and 288.9 eV are assigned to the oxygen bound species C–O and O–C O, respectively [33,34]. No C 1s peak at 281 eV (Ti–C bond) [35] is
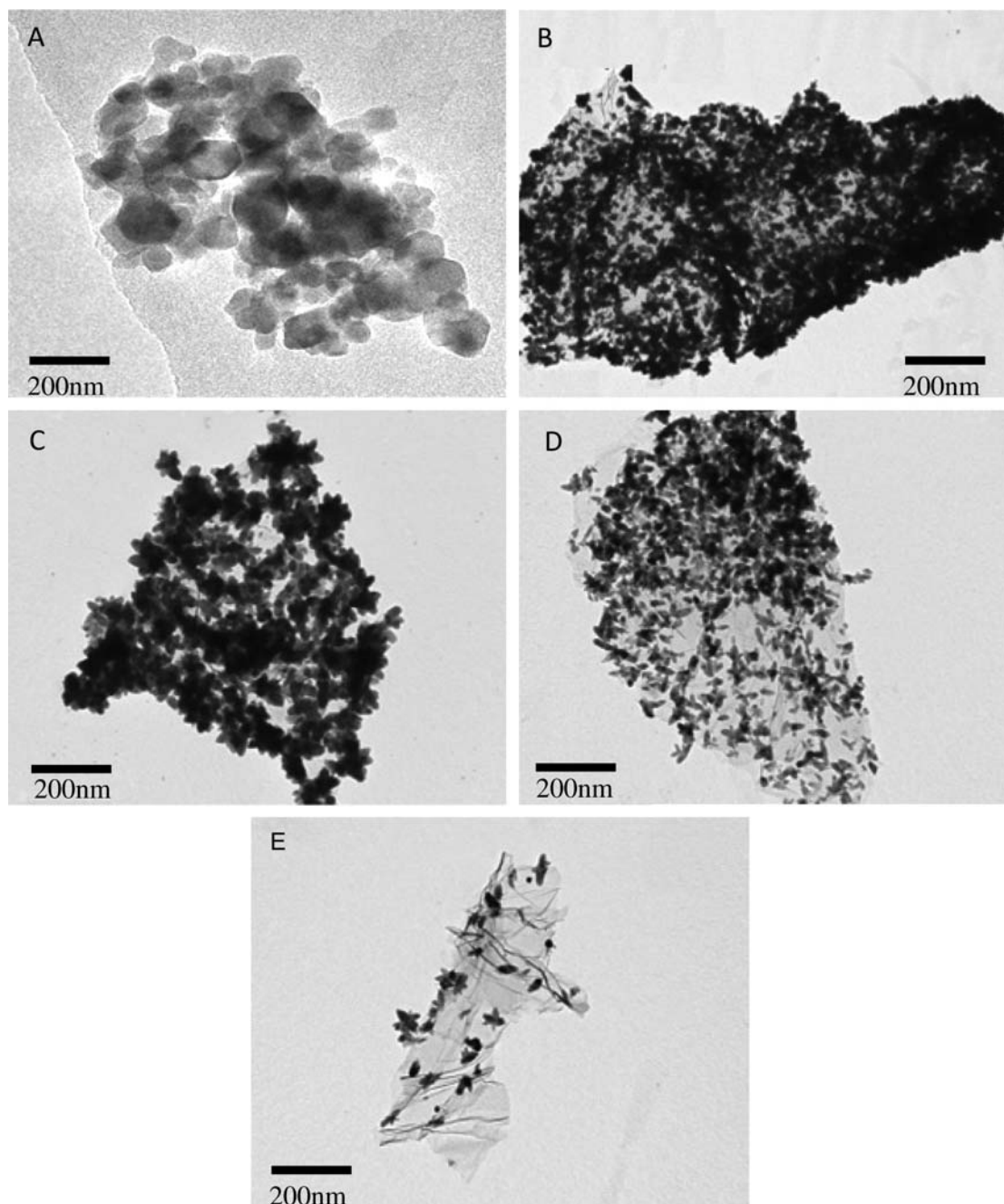
Fig. 5. TEM images of TiO$_2$–RGO composite formed with various GO wt.%: (A) zero, (B) 0.4, (C) 0.8, (D) 1.2, (E) 1.4.

observed, and the chemical environments for Ti and O are not changed, strongly suggesting that carbon atom does not directly enter into bulk TiO$_2$ lattice. This is not expected as many conventional C-doped TiO$_2$ is synthesized at temperatures higher than 600° C [35–37]. Under crystallization conditions used herein, it is thought that TiO$_2$ is grafted onto the graphene layers via C–O–Ti bond, with such structure favoring the desired charge transfer upon light

excitation [38]. C–O–Ti bond extends the light absorption to longer wavelengths.

The nitrogen adsorption/desorption isotherms of the prepared materials are type IV with an H$_2$ hysteresis loop, which is a representative characteristic of mesoporous materials (Fig. 7). As shown in Fig. 7, the N$_2$-adsorbed amount of TiO$_2$ decreased significantly compared with GT composites. The corresponding textural parameters are summarized in Table 1. After
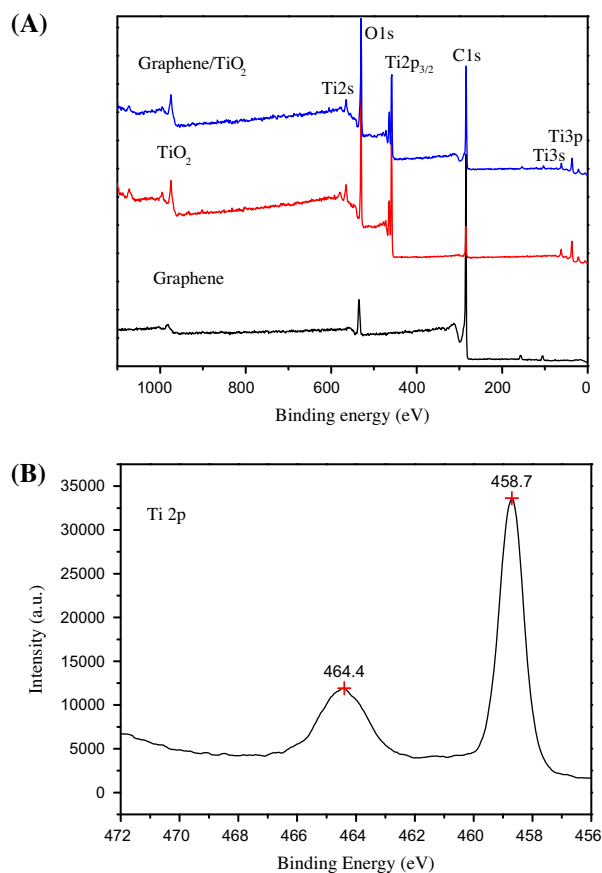
(A)

(B)

Fig. 6. (A) XPS survey spectra of graphene, TiO_2 and graphene@TiO_2. (B) High resolution Ti 2p XPS spectra of TiO_2.
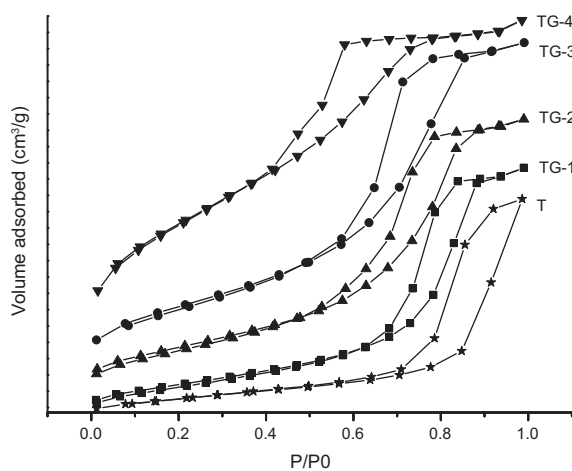

Fig. 7. N_2 adsorption and desorption isotherm of TiO_2 and TiO_2–RGO Composite formed with various GO wt.%.

the introduction of graphene absorbed into the TiO_2 matrix, showed significant increase in pore diameter, pore volume, and BET surface area. In the five

prepared samples, the TG-3 exhibited the largest pore diameter and pore volume, and the TG-3 showed the highest BET surface area.

The UV–vis absorption spectra of TiO_2, TG-1, TG-2, TG-3 and TG-4 are shown in Fig. 8. The sharp characteristic absorption peak at 390 nm indicates the presence of good crystalline and impurity suppressed TiO_2 nanostructures. It is observed that the absorbance of TiO_2–RGO composite increases even in visible light region with the increase of RGO content. Such an increase in absorbance may be due to the absorption contribution from RGO, the increase of surface electric charge of the oxides and the modification of the fundamental process of electron-hole pair formation during irradiation [39]. In addition, the red shift in the absorption edge of TiO_2–RGO composite obtained by extrapolating the linear portion of the curve to zero absorbance as compared to pure TiO_2 is ascribed to the chemical bonding between semiconductor photocatalyst and RGO. Therefore, the presence of RGO in TiO_2 can increase the light absorption

Table 1
Textural parameters and band gap energy of the TiO_2 and RGO- TiO_2 composites

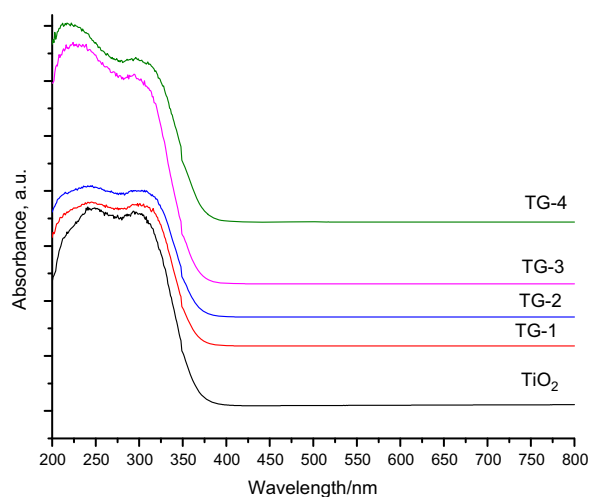| Sample	Vp $(cm^3 g^{-1})$	S_{BET} $(m^2 g^{-1})$	Band gap energy, eV
TiO_2	0.20	90	3.17
TG-1	0.31	150	2.92
TG-2	0.36	161	2.66
TG-3	0.43	173	2.40
TG-4	0.32	163	2.23

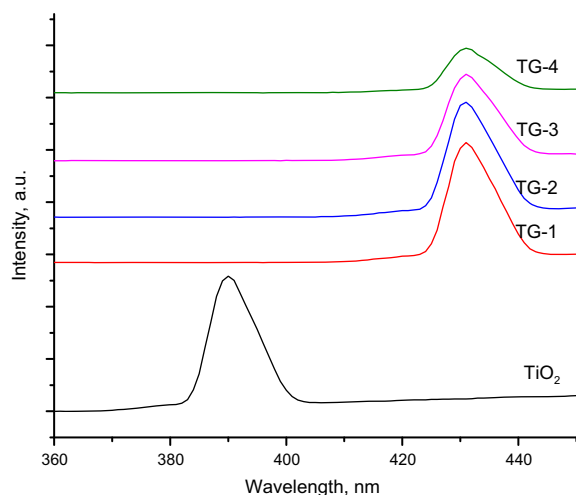Fig. 8. UV–vis absorption spectra of TiO_2 and TiO_2–RGO composite formed with various GO wt.%.

Fig. 9. PL spectra of TiO₂ and TiO₂–RGO composite formed with various GO wt.%.

Fig. 10. Photocalytic degradation of GB by TiO₂ and TiO₂–RGO composite formed with various GO wt.%.

intensity and range, which is beneficial to the photo-catalytic performance. It can be seen from Table 1 and Fig. 8 that the absorption edge of photocatalyst, or the band gap energy, changed with the GO wt.%. The band gap energy of the composites photocatalyst decreased with the increasing GO wt.%.

Fig. 9 shows PL spectra of TiO₂, TG-1, TG-2, TG-3 and TG-4. As compared with the spectrum of pure TiO₂, the PL peak of TiO₂–RGO composite displays a red shift, which is consistent to the result of UV–vis absorption spectra. Furthermore, the introduction of RGO decreases excitonic PL intensity, which indicates that the recombination of photo-induced electrons and holes in TiO₂ can be effectively inhibited in the composite.

3.2. Photocatalytic activity

The photocatalytic activities of TiO₂ and G-TiO₂ composites (TG1–TG4) was measured by the photodeg-radation of GB in gas phase under visible light irradia-tion. It was clear from Fig. 10 a photocatalytic activity of TiO₂ is low, only 5% of GB was degraded. The photo-degradation activity of G-TiO₂ composites (TG1–TG4) were significantly enhanced compared with TiO₂. This indicated that the interactions between graphene and TiO₂ led to the improvement of the photocatalytic activ-ity. Conduction band position of TiO₂ is 3 eV (using vacuum level as a reference), and the work function of graphene is calculated to be 4.42 eV, so graphene can accept conduction band electrons from TiO₂. Under excitation, the conduction band electrons of TiO₂ can be transferred to graphene, and the recombination of photo-generated electron-hole pairs was efficiently
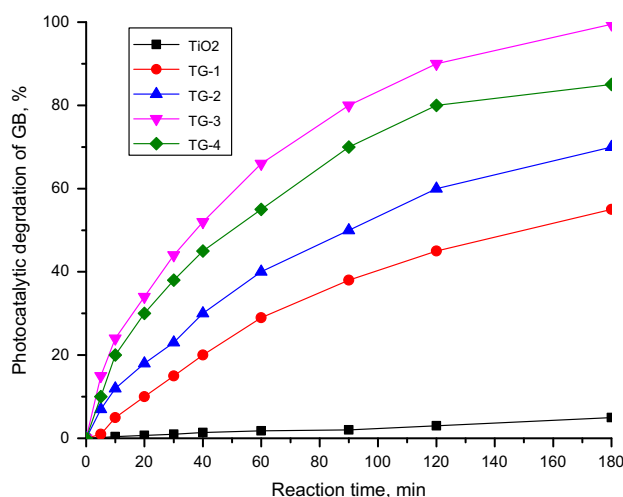
retarded. From this point, the improvement in photo-catalytic activity of G-TiO₂ composites is imaginable. Furthermore, in the G-TiO₂ composites (TG-1–TG-4), the amount of graphene is paramount in determining the photocatalytic activity. From TG-1 to TG-2, the pho-tocatalytic activity for GB was gradually increased, and TG-3 demonstrated the maximized photocatalytic activ-ity, about 99.9% of GB was decomposed in 180 min, dramatically higher than TiO₂ catalyst. This implies that, in TG-1 and TG-2, with the amount of GO in the reaction system is lower than 3 wt.%, the insufficient amount of GO cannot control the homogeneously scat-tering of all the TiO₂ particles, partial TiO₂ particles aggregated or exhibited larger size, which could not effectively interact with graphene, this portion exhibits a lower activity, hinder the overall activity of photocat-alyst. The increment of GO in the reaction system led to better dispersity and smaller particles size of TiO₂ on graphene sheets, the more efficient interactions between graphene and TiO₂ resulted in the retard of electron-hole pairs recombination, so the enhanced of photocata-lytic activity was obtained. With the further increment of GO in the reaction system (over 3 wt.%), the photo-catalytic activity of G- TiO₂ composite (TG-4) decreased. This is also reasonable because the insuffi-cient amount of TiO₂ in the G-TiO₂ composites cause a decrease of the transferred electrons from excitation sta-ted TiO₂, so that reduced the photocatalytic activity.

It is known that during photocatalysis, the light absorption and the charge transportation and separa-tion are crucial factors [28]. The enhancement of the photocatalytic performance should be ascribed to the increase of the light absorption intensity and range, and the reduction of electron-hole pair recombination in

TiO_2 with the introduction of graphene in the composite, which can be confirmed from absorption and PL measurements. However, when the graphene content is further increased above its optimum value, the photocatalytic performance deteriorates. This is ascribed to the following reasons: (i) graphene may absorb some UV light and thus there exists a light harvesting competition between TiO_2 and RGO with the increase of RGO content, which lead to the decrease of the photocatalytic performance [39]; (ii) the excessive RGO can act as a kind of recombination center instead of providing an electron pathway and promote the recombination of electron-hole pair in RGO [40].

The photo-stability of TG-3 by investigating its photocatalytic performance under visible light irradiation with three times of cycling uses was studied. It can be seen that the recycled use of TG-3 does not conspicuously affect its photocatalytic activity thrice. Apparently, the composite is stable under the studied conditions.

4. Conclusions

TiO_2–RGO composites are successfully synthesized via UV-assisted photocatalytic reduction of GO by TiO_2 nanoparticles in ethanol. The experimental results indicate that (i) TiO_2–RGO composites exhibit a better photocatalytic performance than pure TiO_2; (ii) the photocatalytic performance of TiO_2–RGO is dependent on the proportion of RGO in the composite and TiO_2–RGO composite with 3.0 wt.% RGO achieves a highest GB removal rate of 99.5%; (iii) the enhanced photocatalytic performance is ascribed to the increased light absorption intensity and range as well as the reduction of photoelectron-hole pair recombination in TiO_2 with the introduction of RGO.

References

[1] Mehdi Shirzad Siboni, Mohammad-Taghi Samadi, Jae-Kyu Yang, Seung-Mok Lee, Photocatalytic removal of Cr(VI) and Ni(II) by UV/TiO_2: Kinetic study, Desalin. Water Treat. 40 (2012) 77–83.

[2] Niyaz Mohammad Mahmoodi, Mokhtar Arami (Iran), Laboratory studies and CFD modeling of photocatalytic degradation of colored textile wastewater by titania nanoparticles, Desalin. Water Treat. 1 (2009) 312–317.

[3] Yusuke Nakaoka, Hideyuki Katsumata, Satoshi Kaneco, Tohru Suzuki, Kiyohisa Ohta (Japan), Photocatalytic degradation of diazinon in aqueous solution by platinized TiO_2, Desalin. Water Treat. 13 (2010) 427–436.

[4] U.I. Gaya, A.H. Abdullah, Heterogeneous photocatalytic degradation of organic contaminants over titanium dioxide: a review of fundamentals, progress and problems, J. Photochem. Photoboil. A. 9 (2008) 1–12.

[5] G. Li, C. Liu, Y. Liu, Different effects of cerium ions doping on properties of anatase and rutile TiO_2, Appl. Surf. Sci. 253 (2006) 2481–2486.

[6] A. Kumar, A.K. Jain, Photophysics and photochemistry of colloidal CdS–TiO_2 coupled semiconductors–photocatalytic oxidation of Indole, J. Mol. Catal. A: Chem. 165 (2001) 265–273.

[7] X.-H. Xia, Z.-J. Jia, Y. Yu, Y. Liang, Z. Wang, L.L. Ma, Preparation of multi-walled carbon nanotube supported TiO_2 and its photocatalytic activity in the reduction of CO_2 with H_2O, Carbon 45 (2007) 717–721.

[8] M.R. Hoffmann, S.T. Martin, W.Y. Choi, D.W. Bahnemann, Environmental applications of semiconductor photocatalysis, Chem. Rev. 95 (1995) 69–96.

[9] W.D. Wang, P. Serp, P. Kalck, J.L. Faria, Visible light photodegradation of phenol on MWNT–TiO_2 composite catalysts prepared by a modified sol–gel method, J. Mol. Catal. A: Chem. 235 (2005) 194–199.

[10] G. Pyrgiotakis, S.H. Lee, W.M. Sigmund, Advanced photocatalysis with anatase nano-coated multi-walled carbon nanotubes, M.R.S. Spring Meeting, San Francisco, CA, 2005.

[11] K. Woan, G. Pyrgiotakis, W. Sigmund, Photocatalytic carbon-nanotube–TiO_2 composites, Adv. Mater. 21 (2009) 2233–2239.

[12] A.K. Geim, K.S. Novoselov, The rise of graphene, Nat. Mater. 6 (2007) 183–191.

[13] R. Pasricha, S. Gupta, A.K. Srivastava, A facile and novel synthesis of Ag- graphene-based nanocomposites, Nano Lett. 7 (2007) 3394–3398.

[14] J.T. Robinson, F.K. Perkins, E.S. Snow, Z.Q. Wei, P.E. Sheehan, Reduced graphene oxide molecular sensors, Nano Lett. 8 (2008) 3137–3140.

[15] R. Arsat, M. Breedon, M. Shafiei, P.G. Spizziri, S. Gilje, R.B. Kaner, K. Kalantarzadeh, W. Wlodarski, Graphene-like nanosheets for surface acoustic wave gas sensor applications, Chem. Phys. Lett. 467 (2009) 344–347.

[16] S. Stankovich, D.A. Dikin, G.H.B. Dommett, K.M. Kohlhaas, E.J. Zimney, E.A. Stach, R.D. Piner, S.T. Nguyen, R.S. Ruoff, Graphene-based composite materials, Nature 442 (2006) 282–286.

[17] B. Seger, P.V. Kamat, Electrocatalytically active graphene–platinum nanocomposites. Role of 2-D carbon support in PEM fuel cells, J. Phys. Chem. C 113 (2009) 7990–7995.

[18] O. Akhavan, E. Ghaderi, A. Esfandiar, Wrapping bacteria by graphene nanosheets for isolation from environment, reactivation by sonication, and inactivation by near-infrared irradiation, J. Phys. Chem. B 115 (2011) 6279–6288.

[19] T.A. Saleh, M.A. Gondal, Q.A. Drmosh, Preparation of a MWCNT/ZnO nanocomposite and its photocatalytic activity for the removal of cyanide from water using a laser, Nanotechnology 21 (2010) 495705–495713.

[20] S. Wang, X.L. Shi, G.Q. Shao, X.L. Duan, H. Yang, T.G. Wang, Preparation, characterization and photocatalytic activity of multi-walled carbon nanotube supported tungsten trioxide composites, J. Phys. Chem. Solids 69 (2008) 2396–2400.

[21] W.C. Oh, A.R. Jung, W.B. Ko, Characterization and relative photonic efficiencies of a new nanocarbon/TiO_2 composite photocatalyst designed for organic dye decomposition and bactericidal activity, Mater. Sci. Eng. C 29 (2009) 1338–1347.

[22] W.S. Hummers, R.E. Offeman, Preparation of graphite oxide, J. Am. Chem. Soc. 80 (1958) 1339–11339.

[23] D.C. Marcano, D.V. Kosynkin, J.M. Berlin, A. Sinitskii, Z.Z. Sun, A. Slesarev, L.B. Alemany, W. Lu, J.M. Tour, Improved synthesis of graphene oxide, ACS Nano 4 (2010) 4806–4814.

[24] Y.Y. Liang, H.L. Wang, H.N.S.C. Casalongue, Z. Chen, H.J. Dai, TiO_2 nanocrystals grown on graphene as advanced photocatalytic hybrid materials, Non Res. 3 (2010) 701–705.

[25] O. Akhavan, M. Abdolahad, A. Esfandiar, M. Mohatashamifar, Photodegradation of graphene oxide sheets by TiO2 nanoparticles after a photocatalytic reduction, J. Phys. Chem. C 114 (2010) 12955–12959.

[26] D.H. Wang, D.W. Choi, J. Li, Z.G. Yang, Z.M. Nie, R. Kou, D.H. Hu, C.M. Wang, L.V. Saraf, J.G. Zhang, I.A. Aksay, J. Liu, Self-assembled TiO_2–graphene hybrid nanostructures for enhanced Li-ion insertion, ACS Nano 3 (2009) 907–914.

[27] C. Chen, W.M. Cai, M.C. Long, B.X. Zhou, Y.H. Wu, D.Y. Wu, Y.J. Feng, Synthesis of visible-light responsive graphene oxide/TiO_2 composites with p/n heterojunction, ACS Nano 4 (2010) 6425–6432.

[28] H. Zhang, X.J. Lv, Y.M. Li, Y. Wang, J.H. Li, P_{25}-graphene composite as a high performance photocatalyst, ACS Nano 4 (2010) 380–386.

[29] Y.H. Zhang, Z.R. Tang, X.Z. Fu, Y.J. Xu, TiO_2–graphene nano-composites for gas-phase photocatalytic degradation of volatile aromatic pollutant: Is TiO_2–Graphene truly different from other TiO_2–carbon composite materials? ACS Nano 4 (2010) 7303–7314.

[30] H.A. Becerril, J. Mao, Z. Liu, R.M. Stoltenberg, Z. Bao, Y. Chen, Evaluation of solution-processed reduced graphene oxide films as transparent conductors, ACS Nano 2 (2008) 463–470.

[31] G.M. An, W.H. Ma, Z.Y. Sun, Z.M. Liu, B.X. Han, S.D. Miao, Z.J. Miao, K.L. Ding, Preparation of titania/carbon nanotube composites using supercritical ethanol and their photocatalytic activity for phenol degradation under visible light irradiation, Carbon 45 (2007) 1795–1801.

[32] N.P. Zschoerper, V. Katzenmaier, U. Vohrer, M. Haupt, C. Oehr, T. Hirth, Analytical investigation of the composition of plasma-induced functional groups on carbon nanotube sheets, Carbon 47 (2007) 2174–2185.

[33] E. Papirer, R. Lacroix, J.-B. Donnet, G. Nanse, P. Fioux, XPS study of the halogenation of carbon black—Part 2. Chlorination, Carbon 33 (1995) 63–72.

[34] W.J. Ren, Z.H. Ai, F.L. Jia, L.Z. Zhang, X.X. Fan, Z.G. Zou, Low temperature preparation and visible light photocatalytic activity of mesoporous carbon-doped crystalline TiO_2, Appl. Catal. B: Environ. 69 (2007) 138–144.

[35] H. Irie, Y. Watanabe, K. Hashimoto, Carbon-doped anatase TiO_2 powders as a visible-light sensitive photocatalyst, Chem. Lett. 32 (2003) 772–773.

[36] T. Tsumura, N. Kojitani, I. Izumi, N. Iwashita, M. Toyoda, M. Inagaki, Carbon coating of anatase-type TiO_2 and photoactivity, J. Mater. Chem. 12 (2002) 1391–1396.

[37] B. Tryba, A.W. Morawski, T. Tsumura, M. Toyoda, M. Inagaki, Hybridization of adsorptivity with photocatalytic activity – Carbon-coated anatase, J. Photochem. Photobiol. A 167 (2004) 127–135.

[38] M. Niederberger, G. Garnweitner, F. Krumeich, R. Nesper, H. Colfen, M. Antonietti, Tailoring the surface and solubility properties of nanocrystalline titania by a nonaqueous in situ functionalization process, Chem. Mater. 16 (2004) 1202–1208.

[39] T.G. Xu, L.W. Zhang, H.Y. Cheng, Y.F. Zhu, Significantly enhanced photocatalytic performance of ZnO via graphene hybridization and the mechanism study, Appl. Catal. B: Environ. 101 (2011) 382–387.

[40] G. Zhu, T. Xu, T. Lv, L.K. Pan, Q.F. Zhao, Z. Sun, Graphene-incorporated nanocrystalline TiO_2 films for CdS quantum dot-sensitized solar cells, J. Electroanal. Chem. 650 (2011) 248–251.